



THE UNIVERSITY *of* EDINBURGH

Edinburgh Research Explorer

Unusually complex phase of dense nitrogen at extreme conditions

Citation for published version:

Turnbull, R, Hanfland, M, Binns, J, Martinez-Canales, M, Frost, M, Marqués, M, Howie, RT & Gregoryanz, E 2018, 'Unusually complex phase of dense nitrogen at extreme conditions' Nature Communications, vol. 9, no. 1, 4717. DOI: 10.1038/s41467-018-07074-4

Digital Object Identifier (DOI):

[10.1038/s41467-018-07074-4](https://doi.org/10.1038/s41467-018-07074-4)

Link:

[Link to publication record in Edinburgh Research Explorer](#)

Document Version:

Peer reviewed version

Published In:

Nature Communications

General rights

Copyright for the publications made accessible via the Edinburgh Research Explorer is retained by the author(s) and / or other copyright owners and it is a condition of accessing these publications that users recognise and abide by the legal requirements associated with these rights.

Take down policy

The University of Edinburgh has made every reasonable effort to ensure that Edinburgh Research Explorer content complies with UK legislation. If you believe that the public display of this file breaches copyright please contact openaccess@ed.ac.uk providing details, and we will remove access to the work immediately and investigate your claim.



Unusually Complex Phase of Dense Nitrogen at Extreme Conditions

Robin Turnbull¹, Michael Hanfland², Jack Binns³, Miguel Martinez-Canales¹, Mungo Frost^{1,4},

Miriam Marqués¹, Ross T. Howie³ and Eugene Gregoryanz^{5,3,1,*}

¹ Centre for Science at Extreme Conditions and School of Physics and Astronomy, University of Edinburgh, Edinburgh, UK.

² European Synchrotron Radiation Facility, Grenoble, France.

³ Center for High Pressure Science & Technology Advanced Research, Shanghai, China.

⁴ SLAC National Accelerator Laboratory, Menlo Park, California, USA.

⁵ Key Laboratory of Materials Physics, Institute of Solid State Physics, Chinese Academy of Sciences, Hefei, China.

*e-mail: e.gregoryanz@ed.ac.uk

Nitrogen exhibits an exceptional polymorphism under extreme conditions, making it unique amongst the elemental diatomics and a valuable testing ground for experiment-theory comparison. Despite attracting considerable attention, the structures of many high-pressure nitrogen phases still require unambiguous determination. Here we report the structure of the elusive high-pressure high-temperature polymorph ι -N₂ at 56 GPa and ambient temperature, determined by single crystal X-ray diffraction, and investigate its properties using *ab initio* simulations. We find that ι -N₂ is characterised by an extraordinarily large unit cell containing 48 N₂ molecules. Geometry optimisation favours the experimentally determined

ι -N₂ structure and density functional theory calculations find ι -N₂ to have the lowest enthalpy of the molecular nitrogen polymorphs for which the structures are known between 30 and 60 GPa. The results demonstrate that very complex structures, similar to those previously only observed in metallic elements, can become energetically favourable in molecular systems at extreme pressures and temperatures.

Introduction

Extreme-conditions research has uncovered a new regime of complex structures in elemental materials which, counter-intuitively, deviate from simple close packing with the application of pressure. This pressure-induced complexity has previously been exemplified by the structural diversity observed in light alkali and alkaline earth metals^{1–3}. In contrast, such complex, large volume structures have neither been observed, nor have they been predicted, in elemental simple-molecular systems. The nitrogen molecule is used to explore high-pressure phenomena in experimental and theoretical extreme-conditions research because its significant polymorphism makes it unique amongst diatomic elements. Since the first cryogenic experiments of the early 20th century, 15 unique phases of solid nitrogen have been reported over a wide range of pressures and temperatures, including: 12 molecular phases^{4–12}, two non-molecular phases^{13, 14} and an amorphous state¹⁵, as well as numerous predicted structures^{16–20}. The majority of the phases were detected through spectroscopic techniques, which, although useful for providing structural ‘fingerprints’, do not reveal the underlying crystal structures. Consequently, the structures of many of the nitrogen phases remain unknown despite experimental efforts, due primarily to challenges associated with producing and analysing single-crystal samples in the geometrically constrained environment of diamond anvil cells (DACs).

The pressure-temperature (P - T) phase and reaction diagram of nitrogen (illustrated in Fig. 1a) has been a focus-point in high pressure research for the past 15 years since the discovery of the high-temperature high-pressure structures¹² known as ι -N₂ and θ -N₂. The phase which nitro-

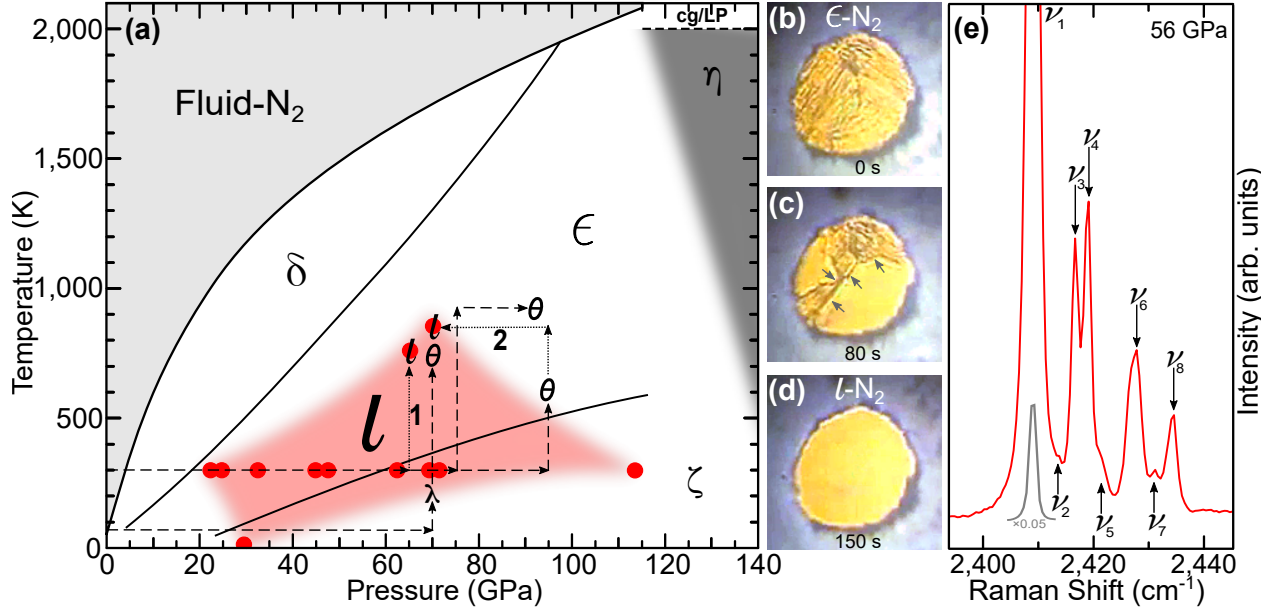


Figure 1 | The nitrogen phase and reaction diagram. (a): The reported P - T paths to the high-temperature molecular phases ι -N₂ and θ -N₂ are shown with dotted and dashed arrows respectively. The red shaded region approximates the known stability field of ι -N₂ based on a combination of our Raman measurements and those of ref. 12. **Path 1:** Isobaric heating of ϵ -N₂ to 750 K at 65 GPa, as performed in this study. **Path 2:** Isothermal decompression of θ -N₂ to 69 GPa at 850 K. P - T paths and data points are taken from refs. 11, 12, 21, 22 which identify the phases through Raman spectroscopy. Black phase-boundaries are based on refs. 21–23. Phases α , β , γ , δ^* , ζ' , κ and λ -N₂ are omitted for clarity. (b-d): Micrographs of the visual changes across the ϵ -N₂ \rightarrow ι -N₂ phase transition. The sample is approximately 60 μ m in diameter and 15 μ m thick. The time from the onset of the phase-transition is shown on each frame. The arrows in (c) indicate the progression of the ϵ -N₂ \rightarrow ι -N₂ phase boundary. (e): Vibrational Raman spectrum of ι -N₂ once recovered to ambient temperature. The inset spectrum (light grey) shows ν_1 scaled by a factor of 0.05 to display it fully.

gen adopts strongly depends on the (P - T) history of the system, and both of the ι -N₂ and θ -N₂ phases are recoverable to ambient temperature and much lower pressures than those required for their synthesis¹² (shown in Fig. 1a). The structures of both ι -N₂ and θ -N₂ have remained unknown since their discovery. The ι -N₂ phase has proved particularly elusive, with only the original study providing experimental data¹² which was limited to Raman and infra-red spectroscopy. Subsequently, one study claimed the production of ι -N₂ after temperature-quenching fluid-N₂ at high-pressure whilst providing no supporting evidence²¹. Other studies have been unable to access ι -N₂ despite replicating the correct P - T conditions²², instead reporting recrystallization of fluid-N₂ into the conventional δ -N₂ and ϵ -N₂ phases without observing ι -N₂ at all²³, thereby casting ambiguity over the P - T path and conditions at which ι -N₂ can be synthesised.

Results

ι -N₂ synthesis and Raman spectra. In this study we have unequivocally synthesised a single crystal of ι -N₂ in a resistively heated DAC from ϵ -N₂ at 65 GPa and 750 K. (See Methods section for further details.) The ϵ -N₂ \rightarrow ι -N₂ transition was initially identified by Raman spectroscopy and visual observation, as shown in Figs. 1b-1e. The transition is characterised by the loss of the ϵ -N₂ ν_1 vibrational mode as shown in the Raman spectra across the synthesis P - T path in Supplementary Figure 1. A video of the phase transition can be seen in Supplementary Movie 1. Typically, ϵ -N₂ has a birefringent appearance which became uniformly smooth on entering the ι -N₂ phase. Phase boundaries between ϵ -N₂ and ι -N₂ were clearly observed moving across the sample chamber (also indicated by arrows in Fig. 1c) and the transition progressed to completion

over several minutes, indicating a kinetically slow phase transition which requires the sustained elevated temperatures generated by resistive heating techniques. This observation may explain why previous studies, which utilised laser heating, have struggled to produce the ι -N₂ phase at the same P - T conditions as the technique suffers from transient and localised peak-temperatures within the sample²⁴. Additionally, Raman spectra of the ι -N₂ to ϵ -N₂ back-transformation on isothermal decompression at ambient temperature (Supplementary Figure 2) show the re-emergence of the ϵ -N₂ ν_1 vibrational mode between 20 – 25 GPa, in agreement with ref. 12.

After recovery to ambient temperature, high resolution Raman spectra were acquired to confirm the synthesis of ι -N₂ (Fig. 1e). In total eight vibrational modes were resolved, all of which originate from molecular N₂ centres. The lowest frequency vibrational mode, ν_1 (2409 cm⁻¹ at 56 GPa), is the most intense by approximately an order of magnitude. The additional higher frequency vibrational modes ($\nu_2 - \nu_8$) are all within 30 cm⁻¹ of ν_1 , describing an unusually complex vibrational spectrum for an elemental molecular system. The lattice modes of ι -N₂, shown in Supplementary Figure 3, appear sharp and well-defined indicating complete orientational ordering which is consistent with the ι -N₂ structure described below.

X-ray crystallography and structure determination. The crystal structure of ι -N₂ was determined by single-crystal synchrotron X-ray diffraction (XRD) at 56 GPa and ambient temperature. The ι -N₂ crystal was of extremely high quality with little strain as evidenced by the very well defined reflections shown in Fig. 2. The data were integrated to a resolution limit of 0.6 Å with an excellent low $R_{int} = 0.0342$ for a total of 1276 (641 unique) reflections. Details of the XRD data collection and refinement are given in Supplementary Table 1 and atomic positions in Supplementary Table 2. The reflections were indexed to a primitive monoclinic lattice with unit-cell dimensions of: $a = 9.899(2)$, $b = 8.863(2)$, $c = 8.726(2)$ Å, $\beta = 91.64(3)^\circ$ and $V = 765.2(3)$ Å³ at 56 GPa. Systematic absence analysis unambiguously indicates the space group is $P2_1/c$ and previously proposed structures can be discarded²⁵. Projections of the refined ι -N₂ crystal structure are shown in Fig. 3. The unit cell is by far the largest observed for any elemental diatomic phase, containing 12 crystallographically unique N₂ molecules, giving a total of 48 N₂ molecules per unit cell. The refined N-N bond lengths are all typical for molecular nitrogen, and the e.s.d.s on the bond lengths and atomic positions (given in Supplementary Table 3) are also low, giving further confidence in the model. For comparison, the next largest nitrogen unit cells belong to ϵ -N₂ and δ^* -N₂, which contain 24 and 16 molecules respectively^{6,10}. The ι -N₂ unit cell is nearly tetragonal about the a axis, with b and c differing by 0.127(2) Å. Of the 48 molecules in the unit cell, 12 are oriented primarily along the a axis (shown in red) and the remaining 36 are layered in the bc plane (shown in blue in Figure 3). Each unit cell contains eight layers, half of which contain axial molecules, with interlayer distances varying between 1.1720(2) and 1.2639(3) Å depending upon the orientation of the axial molecules in the containing layer.

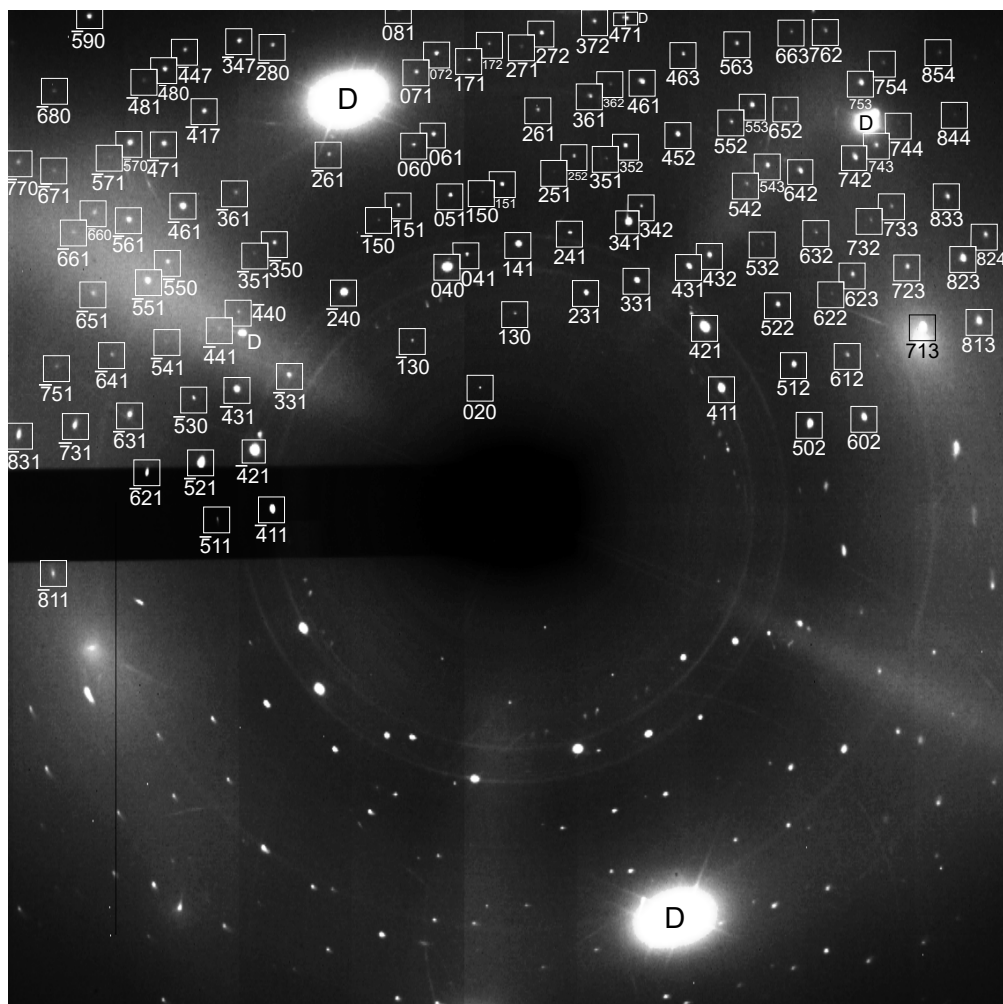


Figure 2 | Single crystal X-ray diffraction pattern of ν -N₂ at 56 GPa. The data were collected over a 56° scan range upon quenching the sample to ambient temperature. Squares mark nitrogen reflections with the given *hkl* indices. Diamond reflections are labelled with the letter *D*. Indices are not shown on the lower half of the image plate to clearly display the quality of the raw data.

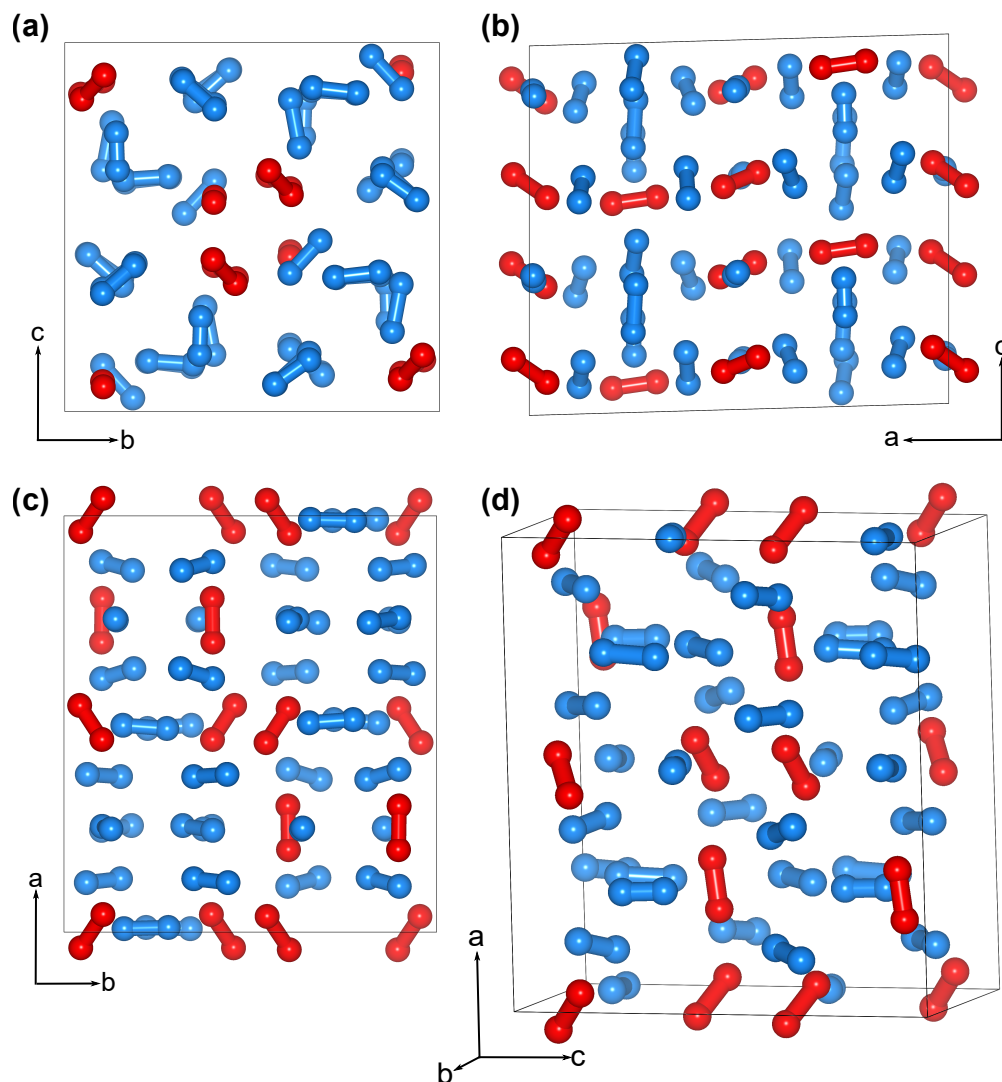


Figure 3 | The refined crystal structure of ι -N₂. (a-c): Projections along the a , b and c axes respectively. (d): A perspective projection of the unit cell. Layered N₂ molecules are shown in blue and oriented molecules are shown in red. Supplementary crystallographic data for the ι -N₂ structure can be obtained free of charge from The Cambridge Crystallographic Data Centre, under deposition number CCDC 1869044.

Density functional theory (DFT) calculations. The refined ι -N₂ structure was analysed using DFT within the standard PBE functional approximation²⁶ and the results found ι -N₂ to be energetically favourable. In geometry optimisation calculations the atomic positions quickly converged to positions, on average, less than 0.005 Å away from the experimentally refined positions, again underlining confidence in the proposed structure. The enthalpy of ι -N₂ was also found to be very competitive (Fig. 4a) and, at the PBE level, better than that of ϵ -N₂ beyond 20 GPa despite ι -N₂ forming at high temperature, suggesting that entropy plays a role in its stability. ι -N₂ was also compared with theoretical low enthalpy candidate high-pressure nitrogen structures proposed by ref. 18 (shown in Fig. 4) which were found to be lower in enthalpy than ι -N₂ by between 10 and 25 meV/atom over the pressure region of interest, however none of the proposed structures of ref. 18 have been observed experimentally. (Note that although the ‘ $P2_1/c$ -candidate’ of ref. 18 shares its space group with ι -N₂, it contains only two molecules.) The calculated ι -N₂ volume per atom shows a volume decrease of approximately 2.5% compared to ϵ -N₂ at ambient temperature and 56 GPa (Fig. 4b) which is consistent with a spontaneous high-pressure phase transition such as the one observed here.

The calculated Raman spectrum (Supplementary Figure 4) reproduces the high frequency vibrational structure, with eight active modes, of which the lowest frequency mode is at least an order of magnitude more intense than the others. Additionally, *ab initio* random structure searches (AIRSS) were performed using all available experimental ι -N₂ constraints, such as the lattice parameters, space group (subgroups were allowed), and number of molecules per cell. The details of the searches can be found in the Methods section below. The experimentally observed ι -N₂

structure was yielded twice, and, of the > 3100 structures generated, none had a lower enthalpy than $\iota\text{-N}_2$, with the next best being a purely molecular structure at 26 meV/molecule greater than $\iota\text{-N}_2$. Such a large systems are not typically attempted with contemporary AIRSS techniques due to computational constraints, and it is certainly noteworthy that $\iota\text{-N}_2$ was found despite the large unit cell and weak intermolecular interactions. Unconstrained and partially constrained searches favour polymerization at these pressures, resulting in mixed molecular/non-molecular phases similar to those predicted previously^{20,27}. It is therefore extremely unlikely that the $\iota\text{-N}_2$ structure would have been found without the experimental constraints, thus highlighting the importance of close collaboration between theory and experiment in the search for high-pressure structures.

Discussion

Our study demonstrates that the appearance of complex structures under pressure is not limited only to metallic elements¹⁻³ and raises the intriguing question of whether unusual phases could be expected in other molecular systems at extreme conditions. The pressure induced complexity in many metallic elements has been attributed to *s-p* or *s-d* electronic transfer^{28,29} which is clearly not an applicable stability mechanism in the case of the molecular and insulating $\iota\text{-N}_2$ phase. Therefore, there must be other mechanisms in highly condensed nitrogen which make these very complex configurations favourable. In the ‘disorder-order’ transition from $\delta\text{-N}_2$ to $\epsilon\text{-N}_2$ the N_2 molecules to forego the entropy of their rotational disorder, in favour of occupying less volume, by ordering in certain molecular orientations¹⁰. In the transition from $\epsilon\text{-N}_2$ to $\iota\text{-N}_2$ however, both phases are characterised by rotationally ordered N_2 molecules. So, what drives the ‘order-order’

transition? In this case the transition is thermodynamically favourable because the volume per atom in the unit cell decreases (as seen in Fig. 4b), whilst the configurational entropy increases due to the larger number of molecules in the unit cell. The ϵ -N₂ to ι -N₂ transition is additionally characterised by a rearrangement of the N₂ molecules into layers (as seen in Fig. 3) which may facilitate vibrational resonance coupling, particularly because molecules between layers take a mutually perpendicular orientation³⁰, which could play an important role in kinetic favourability. Our DFT calculations find ι -N₂ to have the lowest enthalpy of the molecular nitrogen polymorphs for which the structures are known between 30 and 60 GPa, which will surely have implications for the nitrogen phase diagram. Although some pioneering structural searches on nitrogen³¹ have been later confirmed by experiment¹³, these structures were elegantly simple and identified by comparison of powder XRD data with calculated patterns. Our study of ι -N₂ shows that in systems with unforeseen complexity, interesting structures could be potentially overlooked without the direction offered by experiment, and that at extreme conditions unusually complex structures may be more energetically favourable in molecular systems. We hope that our results will prompt further investigations into why such complex structures should appear at high pressures in elemental diatomic solids.

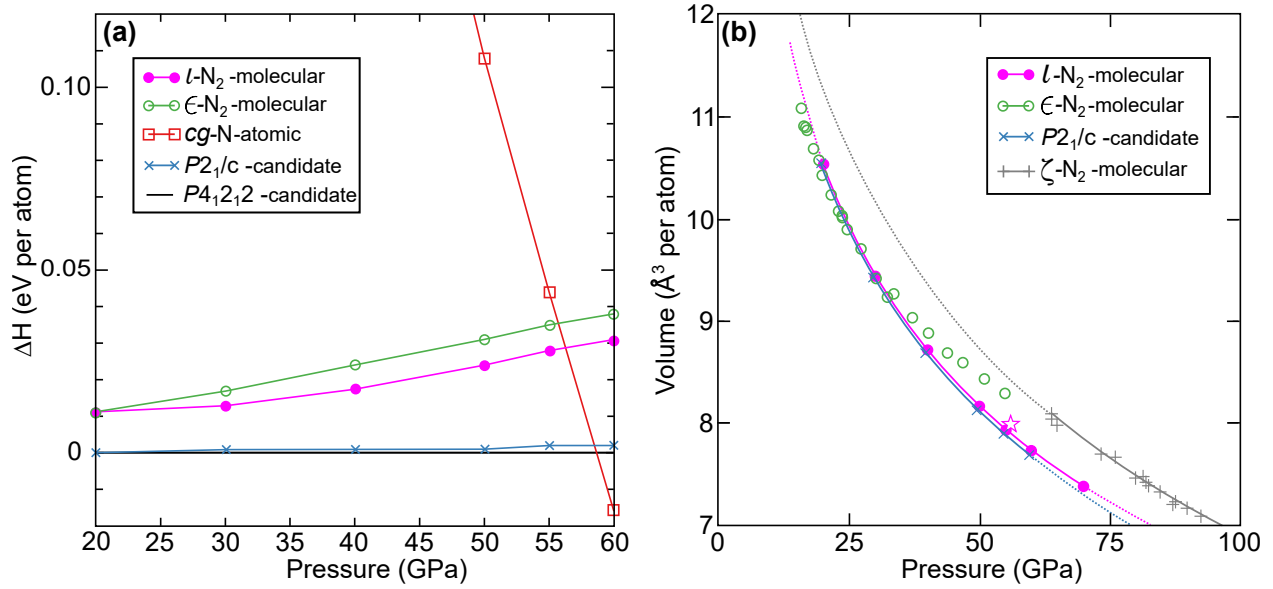


Figure 4 | The calculated enthalpy and volume per atom for the l -N₂ structure. (a): Calculated PBE enthalpy differences with respect to the $P4_12_12$ -candidate structure of ref. 18. The computed enthalpy of l -N₂ is more favourable than ϵ -N₂ above 20 GPa. Polymeric cg -N becomes favourable at 58 GPa, in agreement with previous DFT estimates. **(b):** Calculated volume per atom of l -N₂ and the $P2_1/c$ -candidate structure of ref. 18 plotted with experimental data for ϵ -N₂ and ζ -N₂. The l -N₂ volumes are $\sim 1\%$ larger than the $P2_1/c$ -candidate of ref. 18. The star shows the experimentally determined l -N₂ volume per atom at 56 GPa. The experimental data for ϵ and ζ -N₂ are reproduced from ref. 9 and references therein.

Methods

Sample preparation — Research-grade nitrogen ($> 99.9995\%$ purity, obtained from BOC) was condensed at 77 K and loaded into symmetric DACs equipped with built-in graphite resistive-heaters. Wide opening seats with Boehler-Almax diamonds were used to allow for maximal scattering angle in XRD experiments. Culet sizes were $200\ \mu\text{m}$ and rhenium gaskets were pre-indented to $20\ \mu\text{m}$ prior to loading. Raman spectroscopy was conducted using the 514 nm emission line of an Ar^+ ion laser. Pressure was controlled via a gas-membrane and pressure was determined using the diamond edge scale³². The samples were recovered to ambient-temperature and transported by applying the load of the gas-membrane onto the DAC screws.

X-ray diffraction and structural refinement procedure — Single-crystal XRD data used for refinement were collected at the ID15B beamline at ESRF (Grenoble, France) using a monochromatic beam $\lambda = 0.411\ \text{\AA}$ focused to a spot size of $10 \times 10\ \mu\text{m}$. Data were recorded on a MAR555 flat panel detector. The sample was rotated about ω over a range of 60° in 0.5° increments. The image-plate shown in Fig. 2 was acquired at the Extreme Conditions Beamline (P02.2) at PETRA III (Hamburg, Germany) using a monochromatic beam $\lambda = 0.2889\ \text{\AA}$ focused to a spot size of $4 \times 4\ \mu\text{m}$. Data were recorded on a PerkinElmer XRD 1621 detector. Data were indexed and integrated with CrysAlisPro³³. A total of 1276 reflections were indexed to a monoclinic lattice with unit-cell dimensions $a = 9.899(2)$, $b = 8.863(2)$, $c = 8.726(2)\ \text{\AA}$, $\beta = 91.64(3)^\circ$, $V = 765.2(3)\ \text{\AA}^3$ at 56 GPa. Systematic absence analysis clearly indicated space group $P2_1/c$. Data were integrated to a resolution of $0.6\ \text{\AA}$ with a merged $R_{int} = 0.0342$ for 641 unique reflections, a completeness of

18 %. The crystal was oriented with the c^* axis approximately perpendicular to the diamond culets resulting in a very low data coverage along c^* ($-15 \leq h \leq 15$, $-14 \leq k \leq 13$, $-5 \leq l \leq 4$). The structure was solved by dual-space methods using SHELXT and refinement of the crystal structure was carried out against $|F^2|$ with the SHELXL refinement package^{34,35}. Refinement was limited to an isotropic treatment for all nitrogen atoms, an anisotropic treatment led to refinement instabilities. Rigid bond restraints were applied to all molecular bonds with default estimated standard deviations of 0.004 \AA^2 . Intramolecular bond distance restraints do not improve the fit to the data.

DFT calculations — DFT calculations of energetics and vibrational spectra were performed with CASTEP³⁶ 18.1. Energetics were computed using the default CASTEP 18 ultrasoft pseudopotential, a 700 eV energy cutoff and a k-point grid spacing better than 0.04 \AA^{-1} . In order to estimate the effect of neglected non-local van der Waals interactions, enthalpies were recalculated including Tkatchenko-Scheffler corrections³⁷. The effect is negligible, other than lowering the pressure of the transition to the polymeric *cubic gauche* (*cg*-N) phase. Raman spectra were computed using the DFPT + Finite differences method, using the default CASTEP 18 NC pseudopotentials with a 1250 eV energy cutoff, and a similarly dense k-point grid.

Structure searches — *Ab-initio* evolutionary structural searches for the ι -N₂ structure have been performed with the USPEX³⁸ code and VASP^{39,40}. The initial search space with 1000 structures consisted of atoms and N₂ molecular units. The experimentally proposed $P2_1/c$ symmetry was imposed on some of the searches, but subgroups of lower symmetry such as $P\bar{1}$, Pc and $P2_1$ were also considered. Initial searches with 104 atoms in the unit cell lead to structures $\approx 0.052 \text{ eV/atom}$

higher in enthalpy than those with 96 atoms.

A random structure search was performed with AIRSS⁴¹ and CASTEP 18.1, on the experimental cell with 96 atoms. In total, > 3100 structures were produced. The most favourable searches were those done enforcing initial N₂ molecules and symmetry, generating structures belonging to the $P2_1/c$ space group, as well as its subgroups $P2_1$ and Pc . We were able to reproduce the experimentally refined cell once, and this was the lowest enthalpy structure found under these considerations.

Data availability — Supplementary crystallographic data for the ι -N₂ structure can be obtained free of charge from The Cambridge Crystallographic Data Centre, under deposition number CCDC 1869044, via www.ccdc.cam.ac.uk/structures. All relevant data are available from the corresponding author upon reasonable request.

References

1. Guillaume, C. L., Gregoryanz, E., Degtyareva, O., McMahon, M. I. & Hanfland, M. *et al.* Cold melting and solid structures of dense lithium. *Nat. Phys.* **7**, 211 (2011).
2. Gregoryanz, E., Lundegaard, L. F., McMahon, M. I., Guillaume, C., Nelmes, R. J. & Mezouar, M. Structural diversity of sodium. *Science* **320**, 1054–1057 (2008).
3. Loa, I., Nelmes, R. J., Lundegaard, L. F. & McMahon, M. I. Extraordinarily complex crystal structure with mesoscopic patterning in barium at high pressure. *Nat. Mater.* **11**, 627–632

- (2012).
4. Donohue, J. A refinement of the positional parameter in α -nitrogen. *Acta Crystallogr.* **14**, 1000–1001 (1961).
 5. Schuch, A. F. & Mills, R. L. Crystal Structures of the three modifications of nitrogen 14 and nitrogen 15 at high pressure. *J. Chem. Phys.* **52**, 6000 (1970).
 6. Mills, R. L., Olinger, B. & Cromer, D. T. Structures and phase diagrams of N_2 and CO to 13 GPa by X-ray diffraction. *J. Chem. Phys.* **84**, 2837 (1986).
 7. Hanfland, M., Lorenzen, M., Wassilew-Reul, C. & Zontone, F. Structures of molecular nitrogen at high pressures. *Rev. High Pressure Sci. Technol.* **7**, 787–789 (1998).
 8. Gregoryanz, E., Goncharov, A. F., Hemley, R. J. & Mao, H.-k. High-pressure amorphous nitrogen. *Phys. Rev. B* **64**, 052103 (2001).
 9. Gregoryanz, E., Goncharov, A. F., Sanloup, C., Somayazulu, M., Mao, H.-k. & Hemley, R. J. High P-T transformations of nitrogen to 170 GPa. *J. Chem. Phys.* **126**, 184505 (2007).
 10. Stinton, G. W., Loa, I., Lundegaard, L. F. & McMahon, M. I. The crystal structures of δ and δ^* nitrogen. *J. Chem. Phys.* **131**, 104511 (2009).
 11. Frost, M., Howie, R. T., Dalladay-Simpson, P., Goncharov, A. F. & Gregoryanz, E. Novel high-pressure nitrogen phase formed by compression at low temperature. *Phys. Rev. B* **93**, 024113 (2016).

12. Gregoryanz, E., Goncharov, A. F., Hemley, R. J., Mao, H.-k., Somayazulu, M. & Guoyin S. Raman, infrared, and x-ray evidence for new phases of nitrogen at high pressures and temperatures. *Phys. Rev. B* **66**, 224108 (2002).
13. Eremets, M. I., Gavriluk, A. G., Trojan, I. A., Dzivenko, D. A. & Boehler, R. Single-bonded cubic form of nitrogen. *Nat. Mater.* **3**, 558–63 (2004).
14. Tomasino, D., Kim, M., Smith, J. & Yoo, C.-s. Pressure-induced symmetry-lowering transition in dense nitrogen to layered polymeric nitrogen (LP-N) with colossal Raman intensity. *Phys. Rev. Lett.* **113**, 1–5 (2014).
15. Goncharov, A. F., Gregoryanz, E., Mao, H.-k., Liu, Z. & Hemley, R. J. Optical evidence for a non-molecular phase of nitrogen above 150 GPa. *Phys. Rev. Lett.* **85**, 1262–1265 (2000).
16. Li, Y., Feng, X., Liu, H., Hao, J. & Redfern, S. *et al.* Route to high-energy density polymeric nitrogen t-N via He-N compounds. *Nat. Commun.* **9**, 722 (2018).
17. Wang, X., Wang, Y., Miao, M., Zhong, X. & Lv, J. *et al.* Cagelike diamondoid nitrogen at high pressures. *Phys. Rev. Lett.* **109**, 175502 (2012).
18. Pickard, C. J. & Needs, R. J. High-pressure phases of nitrogen. *Phys. Rev. Lett.* **102**, 125702 (2009).
19. Ma, Y., Oganov, A. R., Li, Z., Xie, Y. & Kotakoski, J. Novel high pressure structures of polymeric nitrogen. *Phys. Rev. Lett.* **102**, 065501 (2009).

20. Mattson, W. D., Sanchez-Portal, D., Chiesa, S. & Martin, R. M. Prediction of new phases of nitrogen at high pressure from first-principles simulations. *Phys. Rev. Lett.* **93**, 125501 (2004).
21. Goncharov, A. F., Crowhurst, J. C., Struzhkin, V. V. & Hemley, R. J. Triple point on the melting curve and polymorphism of nitrogen at high pressure. *Phys. Rev. Lett.* **101**, 1–4 (2008).
22. Tomasino, D., Jenei, Z., Evans, W. & Yoo, C.-s. Melting and phase transitions of nitrogen under high pressures and temperatures. *J. Chem. Phys.* **140**, 244510 (2014).
23. Weck, G., Datchi, F., Garbarino, G., Ninet, S. & Queyroux, J. A. *et al.* Melting curve and liquid structure of nitrogen probed by x-ray diffraction to 120 GPa. *Phys. Rev. Lett.* **119**, 1–5 (2017).
24. Campbell, A. J. Measurement of temperature distributions across laser heated samples by multispectral imaging radiometry. *Rev. Sci. Instrum.* **79**, 015108 (2008).
25. Katzke, H. & Tolédano, P. Theoretical description of pressure and temperature-induced structural phase transition mechanisms of nitrogen. *Phys. Rev. B* **78**, 064103 (2008).
26. Perdew, J. P. Burke, K. & Ernzerhof, M. Generalized Gradient Approximations Made Simple. *Phys. Rev. Lett.* **77**, 3865 (1996).
27. Hirshberg, B., Gerber, R. B. & Krylov, A. I. Calculations predict a stable molecular crystal of N₈. *Nat. Chem.* **6**, 52 (2014).

28. Skriver, H. L. Crystal structure from one-electron theory. *Phys. Rev. B* **31**, 1909–1923 (1985).
29. Errandonea, D. Boehler, R. & Ross, M. Melting of the alkaline-earth metals to 80 GPa. *Phys. Rev. B* **65**, 1–4 (2002).
30. Scheerboom, M. I. M. & Schouten, J. A. Orientational behavior of solid nitrogen at high pressures investigated by vibrational Raman spectroscopy. *J. Chem. Phys.* **105**, 2553–2560 (1996).
31. Mailhot, C., Yang, L. H., & McMahan, A. K. Polymeric nitrogen. *Phys. Rev. B* **46**, 14419–14435 (1992).
32. Akahama, Y. & Kawamura, H. Pressure calibration of diamond anvil Raman gauge to 410 GPa. *J. Phys. Conf. Ser.* **215**, 012195 (2010).
33. CrysAlispro (red) version 1.171. 38.41, (2010).
34. Sheldrick, G. M. SHELXT - Integrated space-group and crystal-structure determination. *Acta Crystallogr. A* **71**, 3–8 (2014).
35. Sheldrick, G. M. Crystal structure refinement with SHELXL. *Acta Crystallogr. C: Struct. Chem.* **71**, 3–8 (2015).
36. Clark, S. J. *et al.* First principles methods using CASTEP. *Z. Kristallogr.* **220**, 567–570 (2005).
37. Tkatchenko, A. & Scheffler, M. Accurate Molecular van der Waals Interactions from Ground-State Electron Density and Free-Atom Reference Data. *Phys. Rev. Lett.* **102**, 073005 (2009).

38. Oganov, A. R. & Glass, C. W. Crystal structure prediction using *ab initio* evolutionary techniques: Principles and applications. *J. Chem. Phys.* **124**, 244704 (2006).
39. Kresse, G. & Furthmüller, J. Efficient iterative schemes for *ab initio* total-energy calculations using a plane-wave basis set. *Phys. Rev. B* **54**, 211169 (1996).
40. Kresse, G. & Joubert, D. From ultrasoft pseudopotentials to the projector augmented-wave method. *Phys. Rev. B* **59**, 1758 (1999).
41. Pickard, C. J. & Needs, R. J. *Ab initio* random structure searching. *J. Phys. Condens. Matter* **23**, 053201 (2011).

Online Content Supplementary display items are available in the online version of the paper.

Acknowledgements This work is supported by a Leadership Fellowship from the UK Engineering and Physical Sciences Research Council (EPSRC), reference number EP/J003999/1. R.T. acknowledges studentship funding from EPSRC Grants No. EP/L504956/1 and No. EP/M506515/1. M.F. acknowledges DOE FES funding number FWP100182. M.M. acknowledges support from the ERC grant Hecate. MMC and MM are grateful for computational support from the UK national high performance computing service, ARCHER, and the UK Materials and Molecular Modelling Hub, which is partially funded by EPSRC (EP/P020194), for which access was obtained via the UKCP consortium and funded by EPSRC grant ref EP/P022561/1.

We acknowledge the European Synchrotron Radiation Facility for provision of synchrotron radiation facilities at the ID15B beamline. Parts of this research were carried out at the light source

PETRA III at DESY, a member of the Helmholtz Association (HGF), under proposal I-20160268 EC. We would like to thank Konstantin Glazyrin for assistance in using the Extreme Conditions Beamline (P02.2).

Author Contributions R.T., M.F. and E.G. conceived and designed the project. R.T., M.H., J.B., M.F. and R.T.H. conducted the experiments. R.T., M.H., J.B., M.F., M.M.C. and E.G. analysed the data. R.T., J.B., M.M.C., M.F., R.T.H. and E.G. wrote the paper. M.M.C. and M.M. performed the DFT calculations. The authors declare no competing interests.

Author Information Reprints and permissions information is available at www.nature.com/reprints. The authors declare no competing financial interests. Readers are welcome to comment on the on-line version of the paper. Correspondence and requests for materials should be addressed to E.G. (e.gregoryanz@ed.ac.uk).